Neurocomputing 153 (2015) 221–234

Contents lists available at ScienceDirect

Neurocomputing

journal homepage: www.elsevier.com/locate/neucom

Fly visual system inspired artificial neural network for collision detection

Zhuhong Zhang [a,*], Shigang Yue [b], Guopeng Zhang [c,b]

[a] Department of Information and Communication Engineering, College of Big Data and Information Engineering, Guizhou University, 550025 Guiyang, Guizhou, PR China
[b] School of Computer Science, College of Science, University of Lincoln, Lincoln LN6 7TS, UK
[c] Institute of Microelectronics, Department of Microelectronics and Nanoelectronics, Tsinghua University, Beijing 100084, PR China

ARTICLE INFO

Article history:
Received 14 May 2014
Received in revised form
10 November 2014
Accepted 15 November 2014
Communicated by A. Belatreche
Available online 24 November 2014

Keywords:
Fly visual neural systems
Artificial neural network
Collision detection
Collision region
Reichardt correlator

ABSTRACT

This work investigates one bio-inspired collision detection system based on fly visual neural structures, in which collision alarm is triggered if an approaching object in a direct collision course appears in the field of view of a camera or a robot, together with the relevant time region of collision. One such artificial system consists of one artificial fly visual neural network model and one collision detection mechanism. The former one is a computational model to capture membrane potentials produced by neurons. The latter one takes the outputs of the former one as its inputs, and executes three detection schemes: (i) identifying when a spike takes place through the membrane potentials and one threshold scheme; (ii) deciding the motion direction of a moving object by the Reichardt detector model; and (iii) sending collision alarms and collision regions. Experimentally, relying upon a series of video image sequences with different scenes, numerical results illustrated that the artificial system with some striking characteristics is a potentially alternative tool for collision detection.

© 2014 Elsevier B.V. All rights reserved.

1. Introduction

The fly's vision system as a bridge of connecting the brain and the visual world is an important information-processing perceptron that perceives and detects spatiotemporal intensity patterns on the retina [1]. Despite a complex internal structure [1–5], it can ensure flies high-speed motion, free navigation, fast object tracking and especially efficient motion adaptation in complex scenes [2], and therefore is a nice bio-inspiration for investigating artificial visual intelligent systems. Visual perception and motion detection are essential and crucial in processing visual information or optic flow that guides much of fly's behavior [6,7]. Studies on such visual system can be categorized into at least four broader types: internal neuronal structure anatomy [1–5]; computational models [8–14]; motion detection and tracking [15–23]; and motion control [19,20]. Especially, visual neuroscientists, who reported many valuable neuronal-based circuit models [1–5], made great efforts to explore intensively internal relationships between neurons, e.g., large monopolar cell (LMC), m_1 and m_2 cells, and lobula plate tangential cell (LPTC). These provide researchers with extremely useful bio-inspirations in resolving complex engineering problems, e.g., object tracking [21–23], flight control [19,20], and colliding avoidance and detection [24–29].

Motion detection is one of the oldest and extremely active topics, involving motion perception, directional selectivity, velocity estimation, and so on. Since insects and in particular flies developed a computationally cheap analysis mechanism used for obstacle avoidance and course control [9], some researchers made great contributions to probing into computational models for motion-directional detection [8–15], while having explored how to use these models to solve engineering problems. EMD, elementary motion detector originally proposed by Hassenstein–Reichardt in 1961 [5] is a classical and vital motion-directional detection model in the fly. On the basis of such popular model, two classes of EMD-based versions, i.e., EMD's extension versions (e.g., [8–12]) and neuronally-based circuit ones (e.g., [13,14]) have recently emerged in large numbers, among which several prominent achievements may handle visual tracking [17,23–25] and robotic motion control [21,26].

Studies on collision detection involve how to develop computational models to detect imminent objects and assume justifying when a collision alarm takes place. When an object appears in the visual field of the fly, the visual inter-neuron will become excitatory. Once the object is close to the fly, the visual inter-neuron system will detect its motion direction, output a high membrane potential, and also make prompt and fast reaction which guides fly's behaviors, e.g., colliding avoidance. These are valuable bio-inspirations for resolving engineering problems, e.g., car or robotic

* Corresponding author.
E-mail addresses: sci.zhzhang@gzu.edu.cn (Z. Zhang), syue@lincoln.ac.uk (S. Yue), zgp12@mails.tsinghua.edu.cn (G. Zhang).

http://dx.doi.org/10.1016/j.neucom.2014.11.033
0925-2312/© 2014 Elsevier B.V. All rights reserved.

collision. However, artificial fly visual collision detection is an entirely new concept. To our knowledge, the recent work on fly-based artificial visual systems has mainly concentrated on EMD-based computational models and internally visual neural structures. It still remains open how fly's internal visual structures can be used to develop computationally visual neural models for collision detection. Then, is the visual neural network of the fly a nice bio-inspiration in solving the problem of collision detection? Can it be utilized to construct artificial visual neural networks for one such problem? Two recent achievements [19,20] have indicated that EMD is a potential tool for detecting the change of optic flow arisen from an imminent object. Particularly, Misserler and Kamangar [23] proposed an artificial neural network (ANN) for detecting and tracking a moving object within the field of view, instead of collision detection. This network can decide the motional position and direction of a moving object, but it requires that the object be small and that some restrictions such as pixel inputs and local detection thresholds hinder its wide application.

In our current work, an artificial visual collision detection system was developed to detect whether and when a collision alarm emerged in complex dynamic environments, in which an artificial fly visual neural network (AFVNN) was proposed to measure the performance characteristics for an object to approach a camera or robot, based on the internal structure of the visual neural system of the fly. It is pointed out that since both AFVNN and ANN all originate from the visual system of the fly; they include the same neural layers – retina, lamina, medulla and lobula. Besides the same neuron division approach used in each of the former two layers, they have different internal structures and applications, due to different design inspirations. On one hand, ANN suits to motion-directional detection and pursuit tracking of a moving object, whereas AFVNN is suitable for collision detection. ANN determines the increment and decrement of activities through on–off nodes in the lamina layer, but AFVNN does so through shunting inhibition; in the medulla layer, ANN decides locally directional motion activities by means of the conventional lateral EMD, a fixed threshold as well as a directional output scheme, but AFVNN determines local motion activities by a two-dimensional synthetic Reichardt correlator without any threshold restriction. Finally, ANN determines the location and direction of a moving target by the winning lobula, but AFVNN outputs a membrane potential in the lobula by summing local motion activities of the neurons in the medulla layer. Additionally, Stafford, Harrison and Yue et al. [28–33] made great contributions to visual neural networks, and developed one basic artificial visual neural network (AVNN). We also emphasize that although AFVNN and AVNN are all suitable for solving the problem of collision detection, they are completely different visual neural networks, due to different bio-inspirations. AVNN bases on the structure of the lobula giant movement detector (LGMD) included in the locust visual neural system, whereas AFVNN is constructed according to the inner structures of the fly visual neural system. On the other hand, their design inspirations are completely different. For example, AFVNN involves in four layers each with the different size of neurons, while a dynamics model is used to present the feature of neuronal output so that its fundamental theory can be investigated helpfully; AVNN also includes four neural layers designed by local lateral inhibition, filter and summation, but each layer is with the same size of neurons.

2. Survey on related work

2.1. Internal neural structure between neurons

Even if anatomizing internal connection between neurons in the visual system of the fly becomes difficult, due to fly's small size, some achievements from several neuroscientists have appeared in the recent literature [1–5], which provides valuable bio-inspirations for researchers to develop available computational models. For example, Clark's group [1] examined two critical pathways in the lamina layer (i.e., L_1 and L_2) that responded preferentially to light and dark moving edges. They demonstrated that the pathways could perform overlapping. Maisak's group [3] studied some response properties of T_4 and T_5 neurons with respect to directional selectivity. A finding was reported that T_4 cells selectively responded to moving brightness increment, but T_5 cells only responded to moving brightness decrements. Eichner's group [5] investigated the internal structure of the fly's motion detection and proposed a four-quadrant-detector related to the classical EMD model.

2.2. Computational models

Computationally fly's visual neural models involve tow boarder types, i.e., EMD-based extension versions and neuronally-based computational models mentioned above. The first type concerns with improving the performance of the classical Reichardt correlator by imposing additional low or high-pass filters [8–12]. Rajesh et al. [8] developed an extension version capable of reducing EMD's dependence on pattern contrast. Such model includes an additional adaptive mechanism, but needs to make further improvements on its feedback gain control scheme so that it can more effectively weaken EMD's dependence on the contrast. Clifford et al. [9] reviewed the reported theoretical and experimental approaches with respect to motion detection, and claimed that adaptation played an important role in motion detection. Higgins and Babies et al. [10,11] developed their augmented EMD models to achieve object tracking and motion-sensitive inhibition. Their results hinted that the proposed models were effective and could explain some electrophysiological phenomena. Meyer et al. [12] investigated how the size and shape of a receptive filed influenced the properties of pattern-dependent response, relying upon several versions of LPTC models. They thought that EMD-based motion detection was subject to uncertainty, and the size and shape of a given receptive field should be matched to the corresponding computational task. On the other hand, the second type of computational model originates from both neuronally-based circuits and the basic Rechardt correlator. This kind of work gets slow progress, because of complexity and difficulty. Several researchers made hard work in studying a few neuronally-based computational models [13,14]. For example, Higgins [13] proposed a model, after analyzing the internal structure between neurons. They asserted that some neurons such as L_1, L_2, T_1, T_5, etc. could constitute small-field elementary motion detector circuits, while these should be integrated with wide-field LPTCs.

2.3. Motion detection and applications

Motion detection on direction and velocity has been being an active research topic in visual neuroscience since 1956 [15–23], in which estimation on position and velocity is a basic and vital branch. Nakamura [15] and Ruffier et al. [16] studied optic flow and direction estimators. They developed efficient motion estimation algorithms to detect changes of optic flow and direction, based on a time-delay Reichardt correlator, and also low and high-pass filters. Their motion sensitivity on the pattern contrast needs to be improved further. In addition, several researchers [17–20] devoted their efforts to augmenting the conventional Reichardt correlator into two-dimensional elaborated EMDs, among which some models as velocity estimators were applied to engineering control [19,20]. On the other hand, EMD-based motion tracking has also been studied preliminarily. Two kinds of visual neural networks from different bio-inspirations, originally proposed by Sun [22] and Misserler [23] respectively were developed to execute object tracking. Sun's network [22] was designed based

on the canonical EMD and BP neural network, solving figure-ground discrimination and target tracking. Misserler's network [23], suitable for directional and positional tracking, was developed based on the internal structure of the fly's vision system, in which the lateral EMD was used to decide local motion direction.

EMD-based collision avoidance and collision detection are a potential and practical branch. The reason of studying collision avoidance is because insects may effectively avoid obstacles in real-world environments [24]. One of the main tasks is to design bio-inspired obstacle avoidance systems that could be used in the guidance of the visually impaired people [25,26]. For example, Badia et al. [26] developed a collision avoidance system to eliminate redundant information on collision avoidance by using an image pre-processing scheme and an edge detection algorithm, in which the EMD block was utilized to compute excitatory signals. However, EMD-based collision detection, different from EMD-based collision avoidance is to provide valuable signals to emphasize imminent collision, for which only a few achievements were reported [28,29]. For example, Stafford et al. [28] integrated their LGMD model with the classical EMD to construct a collision detection system, where the multiplication of the EMD was used to decide the amount of directional excitation after directionally sensitive movement detection.

3. The fly visual system

Visual motion detection in flies starts with the reception of light information, by means of many kinds of photoreceptors arranged in a matrix form. The visual system of the fly is a neural system processing different kinds of visual tasks in either simple or complex environments. It consists of four neural layers – retina, lamina, medulla and lobula [5]. The neurons of each layer only process respective special pieces of information. Retina as the first receptor of the fly receives luminance signals and then transmits them after depolarization. It includes two compound eyes each with lots of arranged ommatidia. Each ommatidium involves in eight photoreceptors, R_1–R_8. These cells detect whether there exists light in the field of view and perceive environmental change. Once light signals with the same optical axis are found by the photoreceptors, they will be transmitted to one column in the lamina after depolarization. Lamina, with a retinotopic and columnar structure, is made up of cartridges arranged in a matrix form. Each cartridge receives a bundle of light along a special optical axis. It includes nine cells, among which five kinds of lamina monopolar cells (LMCs, L_1–L_5) are the main output cells of the lamina. Especially, L_1 and L_2 are the largest LMCs, because they receive most synaptic input from R_1 to R_8. LMCs can perform biologically spatial high-pass filtering and achieve contrast enhancement as a crucial property. When a large variation happens in background intensity, LMCs project their output activities onto the medulla layer after hyperpolarization.

The medulla, with a retinotopic and columnar structure, looks like a small cell tissue with 10 layers M_1–M_{10}, consisting of a large number of columnar neurons and tangential cells which arborize lamina neurons across many medulla columns. Especially, each column involves in lots of local motion-sensitive and direction-selective cells which play an important role in local motion detection. M_1 and M_2 are the main channel subunits to transmit the results of local motion detection to wide-field LPTCs in the posterior regions of the lobula complex and the lobula plate. The lobula complex is comprised of the anterior lobula and the posterior lobula plate with retinotopic and columnar structures, being responsible for receiving input from the medulla and performing the motion detection of whole field. The lobula plate has been studied for a long time in electrophysiology, because it can actively respond to moving stimuli. It contains a numerous of directionally selective motion detection neurons which can perform the motion detection of wide field. Especially, it can bring about the membrane potentials of such neurons, when a moving object appears in the field of view. This might be a nice inspiration for investigating the problem of collision detection, by integrating with motion-directional detection.

4. Artificial fly visual neural network (AFVNN)

Based on fly's internal metaphors of motion detection, we develop a bio-inspired artificial visual neural network for the purpose of collision detection. This neural network, together with a collision detection mechanism, detects when an object approaches the robot or the camera, and also decides when collision alarms are transmitted. It is composed of four neural layers schematically illustrated in Fig. 1 below. The first layer (retina) receives light luminance or gray levels of pixels from successive images and enforces high-pass filtering at the same pixel point. The second layer (lamina) gets brightness from the retina layer and sends the activities of neurons to the third layer (medulla) after shunting inhibition. The third layer outputs local activities of neurons to the last layer (lobula) by means of Reichardt detectors. After summing all local membrane potentials of the neurons and executing shunting inhibition, the last layer produces the whole membrane potential of the network. As related to AFVNN's structure, we give the following detailed designs for the four layers in Fig. 1.

4.1. Retina

The retina layer is composed of $M \times N$ photoreceptors arranged in a matrix form with M rows and N columns, where M and N are multiples of 32. Each photoreceptor corresponds to a pixel point. Since M and N are divisible by 8, these photoreceptors are divided into $m \times n$ blocks in terms of matrix division, where $M=8m$ and $N=8n$. Each block includes 8×8 photoreceptors, where only one block is illustrated in the retina layer in Fig. 1 (see the first layer). Let $L_{ij}(t)$ represent the intensity of pixel (i, j) for an image frame at the moment t, and $p_{ij}(t)$ the averaged luminance signal from the same optical axis received by photoreceptor (i, j) with

$$p_{ij}(t)=\frac{1}{2}(L_{ij}(t)+f(L_{ij})), \quad 1 \le i \le M, \quad 1 \le j \le N, \tag{1}$$

where $f(.)$ denotes a time-delay function.

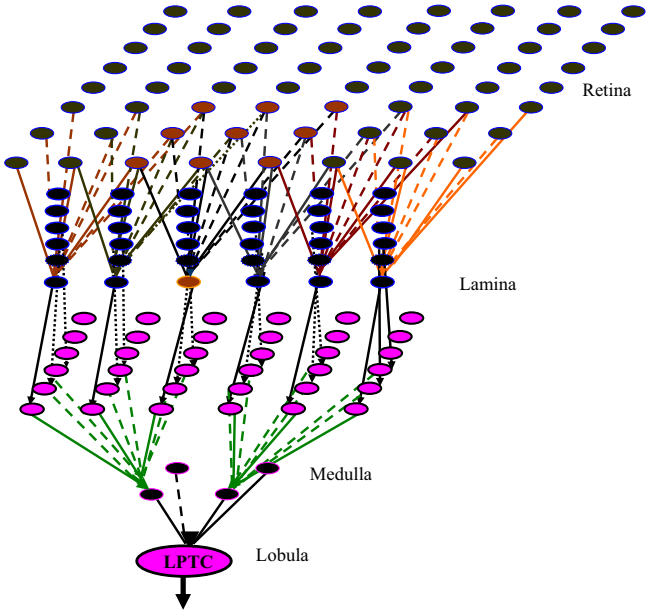

Fig. 1. Artificial fly visual neural network.

4.2. Lamina

The lamina layer consists of two retinotopic sub-layers. The first sub-layer includes $6m \times 6n$ cartridges. Each cartridge receives a convolutional signal produced by 3×3 photoreceptors (see the left hand side between retina and lamina in Fig. 1), and meanwhile relays its activity to a retinotopic counterpart (i.e., LMC) in the second sub-layer after shunting inhibition (see the layer between lamina and medulla in Fig. 1). More precisely, the cartridge of $(6i+k, 6j+l)$ in the first sub-layer connects the sub-block of 3×3 phototreceptors arranged between the $(8i+k)$th and $(8i+k+2)$th rows and between the $(8i+l)$th and $(8i+l+2)$th columns. It collects the light intensity transmitted by the 3×3 phototreceptors in the above sub-block through the following fashion [23]:

$$X_{6i+k,6j+l}(t) = \sum_{u,v=0}^{2} w_{uv}\ p_{8i+k+u,8j+l+v}(t), \tag{2}$$

with $0 \le i < m$, $0 \le j < n$, $0 \le k, l < 6$, where w_{uv} is a weight of input. Basically, Eq. (2) is a neighboring filter used for noise reduction. Let $E_{rs}(t)$ represent the difference between the current light input and the time-delay input at cartidge (r,s) with $0 \le r < 6m$ and $0 \le s < 6n$, namely $E_{rs}(t) = X_{rs}(t) - f(X_{rs})$. In order to detect the response intensity of a cartridge in the sub-layer, an excitatory flow scheme is used to decide the excitatory strength of cartridge (r, s),

$$Y_{rs}(t) = E_{rs}(t) - \frac{1}{8}\sum_{u,v} f(E_{r+u,s+v}),\ \ (-1 \le u, v \le 1) \wedge \neg(u+v=0). \tag{3}$$

Subsequently, all the cartridges send their excitatory flows to their counterparts (LMCs), which can be achieved through the modified shunting inhibition equation [23]:

$$\dot{x}_{rs} = -A_l x_{rs} + (B_l - x_{rs})Y_{rs}, \quad 0 \le r < 6m, \quad 0 \le s < 6n, \tag{4}$$

where A_l is a positive decay coefficient, and B_l represents a positive and maximal activity. Notice that Eq. (4) represents an interconnected dynamic system composed of $6m \times 6n$ equations. We assert that for a given neuron (r, s), if $f(.)$ is a bounded function, x_{rs} changes within $-B_l$ and B_l.

4.3. Medulla

LMCs in the lamina layer project their outputs onto medulla cells by means of synthetic correlators. More precisely, each block of 3×3 LMCs in the lamina layer provides its combinational output to a single medulla cell after using a classical synthetic Reichardt correlator without the limit of threshold schemethetically illustrated in Fig. 2. This way, the medulla layer consists of $6m/3 \times 6n/3$ medulla cells arranged in a matrix form. Note that a single medulla cell, e.g. (p, q), only corresponds to a single block of LMCs arranged between the $3p$th and $(3p+2)$th rows and between the $3q$th and $(3q+2)$th columns in the lamina layer with $0 \le p < 2m$ and $0 \le q < 2n$. For the medulla cell of (p, q), we view the LMC of $(3p+1,3q+1)$ as the center of the LMC block mentioned above. After that, the activity of cell (p, q) can be computed by

$$m_{pq} = \sum_{0 \le u,v \le 2} \left(x_{3p+1,3q+1} f(x_{3p+u,3q+v}) - x_{3p+u,3q+v} f(x_{3p+1,3q+1})\right)^2, (u+v \ne 0). \tag{5}$$

Thereafter, the final potential of motion sensitivity for cell (p, q) is acquired by means of the Sigmoid function:

$$M_{pq} = \frac{1}{1+\exp(-m_{pq})} - 0.5, \quad 0 \le p < 2m, \quad 0 \le q < 2n. \tag{6}$$

4.4. Lobula layer

The lobula layer collects motion-sensitive activities from the medulla layer and outputs its combinational information after shunting inhibition. We calculate the membrane potential of a given PLTC simply through the following equation:

$$\dot{Y}_{lob} = -A_P Y_{lob} + (B_P - Y_{lob})\left(\sum_{p=0}^{2m-1}\sum_{q=0}^{2n-1} M_{pq} - f\left(\sum_{p=0}^{2m-1}\sum_{q=0}^{2n-1} M_{pq}\right)\right), \tag{7}$$

where A_P and B_P are the decay coefficient and the amplitude of variable Y_{lob} resepctively. Note that Y_{lob} ranges within $-B_P$ and B_P theoretically.

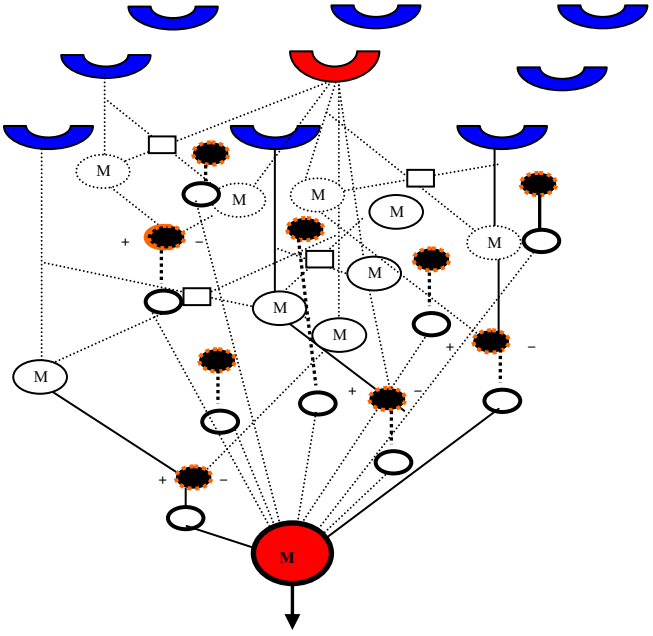

Fig. 2. Synthetic Reichardt correlator.

5. Artificial visual collision detection system (AVCDM)

5.1. Spiking detection mechanism

Based on a given video sequence and AFVNN, an adaptive threshold scheme for collision detection is designed to detect whether a spike appears in the field of view. In other words, let $Y_{lob}(k)$ be the membrane potential acquired after the kth image enters AFVNN, decided by Eq. (7) at the kth step. Define

$$Y(k) = \frac{Y_{lob}(k) - \overline{Y}(k)}{Y_{lob}(k) + \overline{Y}(k)}, \tag{8}$$

where

$$\overline{Y}(k) = \sum_{i=1}^{l} w_i Y_{lob}(k-l-i), \quad w_i = \frac{1-\lambda(k-i)}{\sum_{j=k-l}^{k-1}(1-\lambda(k-j))}, \quad 1 \le i \le l,$$

with step span l and small coefficient λ. Threshold $\sigma_{th}(k)$ is designed as follows:

$$\sigma_{th}(k) = \begin{cases} 0, & Y_{lob}(k) \le 0, \\ Y_{lob}(k) + \tau, & Y_{lob}(k) > 0, \overline{Y}(k) \le 0, \\ |Y(k)| + \tau, & Y_{lob}(k) > 0, \overline{Y}(k) > 0, |Y(k)| > \tau, \\ \tau, & Y_{lob}(k) > 0, \overline{Y}(k) > 0, |Y(k)| \le \tau, \end{cases} \tag{9}$$

with $0 < \tau \le 0.5$. Usually, when the brightness of an object becomes dazzling or conspicuous, a robot or camera will receive a strong stimulus signal and output a large membrane potential, which brings about a spike. We use the spiking mechanism [29] to

detect whether a spike appears in the retinotopic field of view, i.e.,

$$S(k)=\begin{cases}1, & Y_{lob}(k)\geq\sigma_{th}(k),\\ 0, & \text{else},\end{cases} \tag{10}$$

where 1 represents a spike and 0 means no spike.

5.2. Motion-directional detection mechanism

5.2.1. Local motion direction detection

We recall the motion-directional detection model in the medulla layer originally proposed by Missler and Kamangar [23]. Such model can determine the motion direction of a moving object when such object is small and not close to the camera or robot. However, when the edge of the object in the field of view enlarges gradually, the model is difficult in detecting a moving object. In the current work, after this model is improved, the acivities of motion direction are used to integrate with the output of the above network so as to assistantly identify whether to occur conllision. The main improvements includes (i) there is no threshold Γ in the directional inhibition, and (ii) the horizontal and vertical activities are decided respectively by horizontal and vertical projections from differences of activities of pair-wise m_1 cells (see Fig. 3). For a given block composed of 3×3 LMCs in Section 4.3, let m_{1k} be a medulla cell acquired through directional inhibition from the kth LMC to the central one, and $\overline{m}_{1k}$ the opposite. Their potentials are the activities of directional inhibition,

$$m_{1k}=x_0 f(x_k),\quad \overline{m}_{1k}=x_k f(x_0),\quad 1\leq k\leq 8, \tag{11}$$

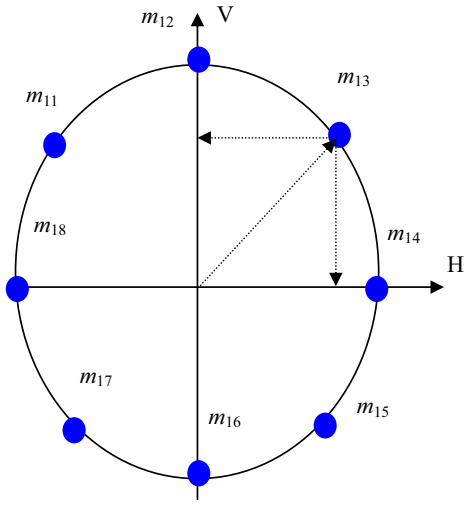

Fig. 3. Local motion-directional detection.

each block produces its horizontal and vertical direction potentials. We next compute the combinational direction potentials of all the blocks presented in the above two groups, of which each is the sum of the absolute values of horizontal and vertical direction potentials for a corresponding block. Finally, the block with the largest combinational direction potential outputs its direction potential vector (X_{lobh}, X_{lobv}) as the directional activity of a moving object.

$$\begin{aligned} m_{2h}&=m_{11}-\overline{m}_{11})\cos\frac{\pi}{4}+(\overline{m}_{13}-m_{13})\cos\frac{\pi}{4}+(\overline{m}_{14}-m_{14})+(\overline{m}_{15}-m_{15})\cos\left(\frac{\pi}{4}\right)+(m_{17}-\overline{m}_{17})\cos\left(\frac{\pi}{4}\right)+(m_{18}-\overline{m}_{18}),\\ m_{2v}&=(m_{11}-\overline{m}_{11})\sin\frac{3\pi}{4}+(\overline{m}_{12}-m_{12})+(\overline{m}_{13}-m_{13})\sin\frac{\pi}{4}+(m_{15}-\overline{m}_{15})\sin\frac{3\pi}{4}+(m_{16}-\overline{m}_{16})+(m_{17}-\overline{m}_{17})\sin\left(\frac{\pi}{4}\right),\end{aligned} \tag{12}$$

where x_k and x_0 are the activities of the kth and the central LMC, respectively. Hence, these m_1 cells project their activities onto a matching m_2 cell through the following equation:
where m_{2h} and m_{2v} denote the horizontal and vertical direction potentials of cell m_2, respectively. At the same way, other 3×3 LMC blocks in the lamina layer above can also obtain the directional potentials of their matching m_2 cells.

5.2.2. Object motion direction detection

As we state in Section 4.3, the medulla layer is composed of medulla cells arranged in a $2m\times 2n$ matrix form, each with a direction potential vector (m_{2h}, m_{2v}) decided by Eq. (12). Since m and n are divisible by 4, we acquire two groups of blocks through one such medulla layer, relying upon the idea of matrix division given by Missler and Kamangar ([23], Fig. 9, pp. 427). The first group is obtained after uniformly dividing the $2m\times 2n$ matrix, including $m\times$ n)/16 blocks each with 8×8 medulla cells. For a given block among them, we can acquire its horizontal and vertical direction potentials $\mathrm{X_{lobh}}$ and $\mathrm{X_{lobv}}$ through the following equations,

$$\dot{\mathrm{X}}_{\mathrm{lobh}}=-A_l\mathrm{X}_{\mathrm{lobh}}+(B_l-\mathrm{X}_{\mathrm{lobh}})(\mathrm{m}_{\mathrm{lobh}}-f(\mathrm{m}_{\mathrm{lobh}})), \tag{13}$$

$$\dot{\mathrm{X}}_{\mathrm{lobv}}=-A_l\mathrm{X}_{\mathrm{lobv}}+(B_l-\mathrm{X}_{\mathrm{lobv}})(\mathrm{m}_{\mathrm{lobv}}-f(\mathrm{m}_{\mathrm{lobv}})), \tag{14}$$

where $\mathrm{m_{lobv}}$ and $\mathrm{m_{lobv}}$ are the sums of horizontal and vertical direction potentials of medulla cells involved in one such block, respectively. Additionally, by uniformly dividing the $2m\times 2n$ matrix but not including rows 1–4 and $2m-3$ to $2m$ and also columns 1–4 and $2n-3$ to $2n$, we get the second group with $((m-4)\times(n-4))/16$ blocks each with 8×8 medulla cells. Based on the same calculation method above,

5.3. Collision detection

Collision alarm depends on the above mechanisms of spiking and motion-directional detection. It is necessary to present a spike in the field of view, when the object is approaching the camera or robot. Additionally, the signs of the horizontal and vertical coordinate values of direction (X_{lobh}, X_{lobv}) for a moving object are important during motion-directional detection, because they can help the collision detection mechanism detect whether collision occurs. Generally speaking, a collision might happen if the direction of the object is located between the third and forth quadrants, and the absolute of the slope of the direction is beyond 1. We introduce an indicator to describe such case given by

$$I_D(k)=\begin{cases}1, & (|X_{lobv}(k)/X_{lobh}(k)|\geq 1)\wedge(X_{lobv}(k)<0),\\ 0, & \text{else}.\end{cases} \tag{15}$$

On the other hand, when an object appears in the field of view and causes some spikes within several time steps, the collision phenomenon might take place. We give another indicator to indicate such case [30],

$$I_P(k)=\begin{cases}1, & \sum_{i=k-S_p}^{k}S(k)\geq N_p,\\ 0, & \text{else},\end{cases} \tag{16}$$

where N_p is a threshold of collision alarm and S_p is the step span with $N_p\leq S_p$. Based on Eqs. (15) and (16), a collision alarm

mechanism is defined by

$$C_{final}^{k}=\begin{cases}\text{True}, & (I_D(k)=1)\wedge(I_P(k)=1),\\ 0, & \text{else}\end{cases}. \tag{17}$$

6. Experimental study

We first display a set of sample videos used in this experiment, and then analyze their characteristics in Section 6.1. AVCDM's performance is analyzed based on the acquired experimental results in Section 6.2. Finally, one competitive visual neural collision detection system is chosen to compare against AVCDM.

6.1. Environmental settings

Throughout this study, all experiments are executed on a Windows XP system with CPU/3.00 GHz and RAM/2 G, and source codes are written in VC++. Each input image frame is with 128×128 pixels, i.e., $M=128$ and $N=128$. Other parameters in AFVNN and AVCDM are adjustable. After trial, we define their parameters as given in Table 1.

In this experiment, three different kinds of test environments are studied, including a total of 10 video sequences (see Fig. 4, below), in which each sequence represents a scene and the field of view is 60°. The first environment involves steel ball movement in the robotic laboratory, including 8 video sequences (see video sequences 1–8) each with 60 frames. Each sequence is generated by a video camera mounted on the turret of a Khepera robot in a robotic laboratory in the process of motion of a ball. The second environment is described by a scene where one pedestrian walks across a highway from right to left, including a video sequence with 119 frames (see video sequence 9). The last environment is illustrated by a video sequence with 222 frames (see video sequence 10), used in car collision detection outdoor. We will extract 5 representative frames for each video sequence except video sequence 10 to represent the performance of a moving object because of the limited space of page, while analyzing in detail what characteristics each video sequence includes.

Video sequences 1 and 2 are arisen from the same scene but different motion fashions. Video sequence 1 emphasizes that a black ball with 95 mm in diameter is moving fast across the field of view from left to right at a speed (0.4–0.5 m/s) but not close to the robot, only taking frames 14, 16, 18, 21 and 23 for example. In one such sequence, the black ball changes its motion direction with time after an initial velocity. For example, the ball moves toward slide up in frame 14 but in frame 16 toward slide down; meanwhile, after being touched a wall suddenly, the ball rebounds off the wall. Conversely, in video sequence 2, the black ball is moving but not bouncing to the robot along the right diagonal line from up to down. Therefore, such motion process gives rise to a difficult issue, i.e., how to decide motion direction. Video sequences 3 and 4 arise from the same background, among which the black ball with 95 mm in diameter is moving from left to right or from the right-up corner to the door at a high velocity. In such two sequences, the ball is far from the robot but in the field of view, and therefore some weak signals can only be captured by the robot. On the other hand, in video sequence 3 the ball is bouncing recurrently between left and right, and thus the robot can easily find the ball. However, in video sequence 4, since the ball is rolling rapidly and away from the scene from the corner to the door, it is difficult that the robot captures some information on the ball, due to visual processing. Video sequences 5–7 are represented by video motion frames, including collusion circumstances. In video sequences 5 and 7, the ball is approaching the robot from the front and leaving the robot from right down to left-up, such two sequences come from different scenes. In video sequence 6, the ball is approaching the right-down corner and leaving along the right-up direction. These sequences all involve collision events. Video sequences 8 and 9 describe that an object moves on the horizontal direction, but display different motion characteristics. In video sequence 8, a black ball is moving from left to right at a high velocity, whereas in video sequence 9, one pedestrian walks across the highway from right to left at a slow velocity, while another pedestrian is also moving aside the highway. In video sequence 10, sample images from video sequences making up a car driving environment. In the front of video images, an inflatable car is used for a collision source. The driving car is translating toward the front at a low or high speed. It rotates anticlockwise or clockwise within frames 50 and 70 continually, while approaching the inflatable car at a high velocity and taking place collision at frame 182.

Table 1
Parameter settings.

A_l	B_l	A_p	B_p	l	τ	S_p	N_p
5	10	2	2	5	0.25	8	5

6.2. Results and discussion

It is pointed out that each of the video sequences includes some clues which the moving object (ball, pedestrian or car) appears in the field of view. Here, we examine whether AVCDM can provide some strong collision signals and send collision alarms. Especially, it is detected whether changes of AFVNN's membrane potentials correspond to the performance of the moving object. Video sequences 1–3 involve in two collision regions respectively, but others only include a collision region respectively. The statistical results are displayed in Table 2. AVCDM's collision detection performance can be known through Figs. 5–7.

Table 2 indicates that AVCDM can correctly find the collision regions for all videos but video sequence 3. In video sequence 3 (see Fig. 4(3)), we notice that the black ball bounces at a high speed during frames 9–24, and thus AFVNN has somewhat high membrane potentials; however, its motion suddenly becomes slow during 24–37, and hence AFVNN can only produce lower membrane potentials; during frames 38–60, the ball rolls slowly, and therefore its activities are low. Through the seventh column in Table 2, AVCDM can find one collision region (frames 21–23), but is difficult in providing collision alarms for frames 24–35; the main reason is because the robot is far from the ball and AFVNN can only receive weak light luminance on the ball. In such case, we think AVCDM can successfully send alarms but only transmit a narrow collision alarm region; in other words, its success rate of collision alarm is 100%, while the success rate of the collision alarm region acquired is defined as 50%.

Based on the artificial visual neural network (AFVNN), AVCDM executes collision detection under the above three different environments. Video sequences 1–8 come from the motion of a black ball at a high or mediate velocity. Graphically, in Fig. 5(1) the membrane potential curve presents AFVNN's output performance that reflects rationally the moving characteristic of the ball in the field of view; in particular, AFVNN produces high membrane potentials over two intervals (frames 12–25 and 27–52), as video sequence 1 includes two collision regions known from Table 2; the threshold curve can correctly identify the two collision regions, as the threshold levels for those frames without collision are always larger than those membrane potentials, namely the threshold curve segments for those collision regions are in order under those membrane potential curve segments; additionally, the short dotted curve presents clearly two collision regions for the ball and

（14） （16） （18） （21） （23）

Video 1. The ball is bouncing up and down at 0.4~0.5m/s from the left-hand side to the right-hand side, keeping an intermediate distance between the ball and the robot.

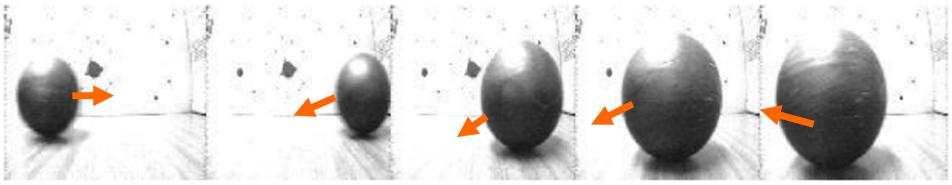

（30） （36） （53） （56） （60）

Video 2. The ball is approaching the robot along the right diagonal from up to down at an intermediate speed.

（10） （13） （16） （19） （30）

Video 3. The ball is bouncing up and down from left to right at a fast velocity.

（31） （34） （37） （40） （49）

Video 4. The ball is moving from the corner to the door at an intermediate velocity.

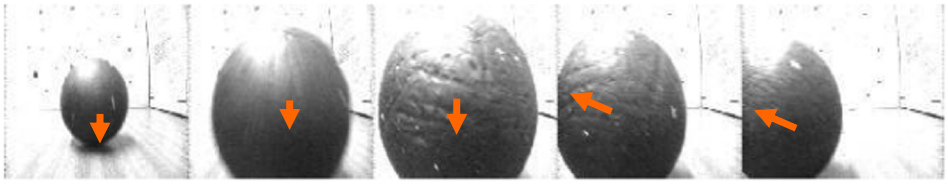

（20） （25） （30） (35) (40)

Video 5. Collsion from the front.

(40) (45) (50) (52) (54)

Video 6. Collsion from the left-up to right-down.

Fig. 4. Ten video sequences each with 5 extracted representative frames. (1) The ball is bouncing up and down at 0.4–0.5 m/s from the left-hand side to the right-hand side, keeping an intermediate distance between the ball and the robot. (2) The ball is approaching the robot along the right diagonal from up to down at an intermediate speed. (3) The ball is bouncing up and down from left to right at a fast velocity. (4) The ball is moving from the corner to the door at an intermediate velocity. (5) Collsion from the front. (6) Collision from the left-up to right-down. (7) Collision from the front. (8) The ball is moving along the horizontal direction. (9) One pedestrian is across the highway. (10) Car motion on the vertical direction.

the robot, which corresponds to the practical scene. At the same way, Fig. 5(2)–(4) hints that AFVNN can also produce rational membrane potentials to explain the motion performance of the ball; correspondingly, AVCDM can also identify correctly the collision regions for video sequences 2 and 4. However, since the moving ball in video sequence 3 is far from the robot but moves in

(40) (45) (50) (54) (54)

Video 7. Collsion from the front.

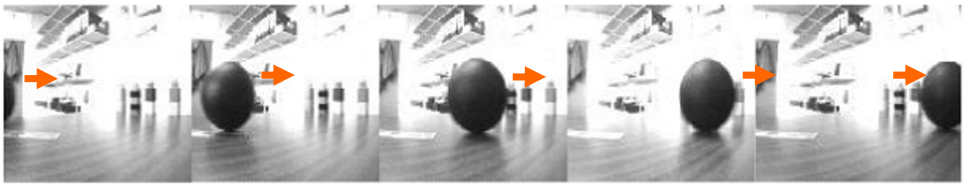

(34) (37) (40) (42) (44)

Video 8. The ball is moving along the horizontal direction.

(5) (10) (30) (35) (40)

Video 9. One pedestrian is across the highway.

（100） （110） （120） （130） (140)

(150) (160) (170) (180) (190)

Video 10. Car motion on the vertical direction.

Fig. 4. (*continued*)

the field of view, AFVNN can only output small membrane potentials (see Fig. 5(3)). This makes the threshold scheme in AVCDM only find a small part of the collision region and also only send a collision alarm signal for the other part (frames 24–35), because of AFVNN's low membrane potentials and the same setting of τ as in the threshold scheme for all test videos.

Fig. 6 takes on the results acquired by AVCDM for video sequences 5–8 each with only one collision region, in which Fig. 6(1)–(4) correspond to the videos in order. The curves of membrane potential and threshold as well as collision regions in Fig. 6 expose clearly AVCDM's characteristics. As associated to Table 2, AVCDM can not only precisely send collision alarm signals, but also correctly determine the collision region for each video sequence.

Video sequence 9 comes from a scene where one person walks across the highway at a slow velocity from left to right. The camera

Table 2
Collision region detection.

Video no.	The total of frames	Object type	Speed type	Practical collision region (frames)	AVCDM's collision region (frames)	Success rate (%)
1	60	Ball	Fast	12–25, 27–52	16–24, 39–46	100
2	60	Ball	Fast	29–36, 48–60	32–39, 52–58	100
3	60	Ball	Fast	13–35	21–23, 31–31	50
4	60	Ball	Fast	33–45	42–47	100
5	60	Ball	Mediate	20–38	26–39	100
6	60	Ball	Mediate	37–54	41–57	100
7	60	Ball	Mediate	40–60	46–60	100
8	60	Ball	Fast	37–43	37–46	100
9	119	Walker	Slow	25–39	31–38	100
10	222	Car	Fast	144–222	165–198	100

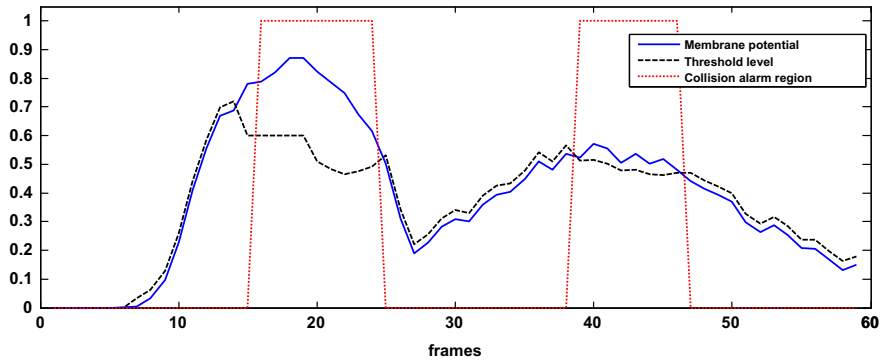

(1) video 1

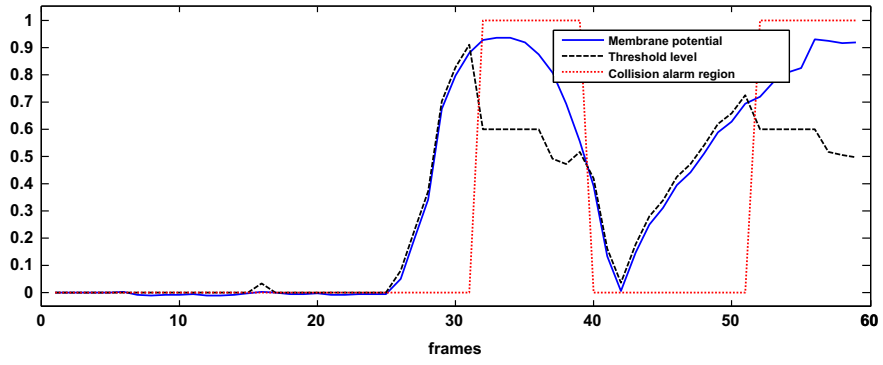

(2) video 2

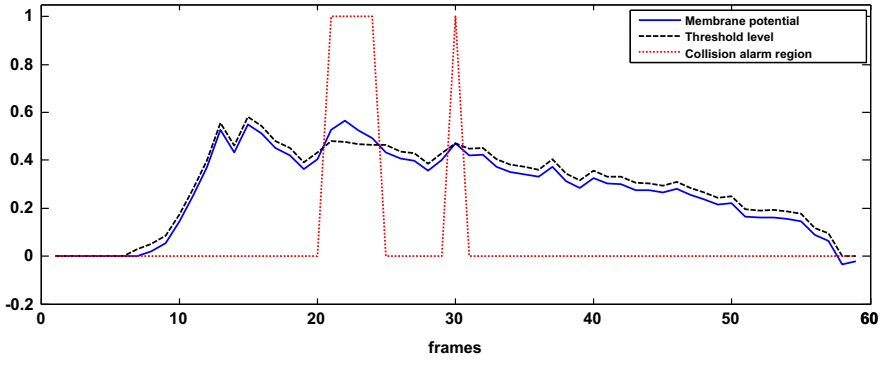

(3) video 3

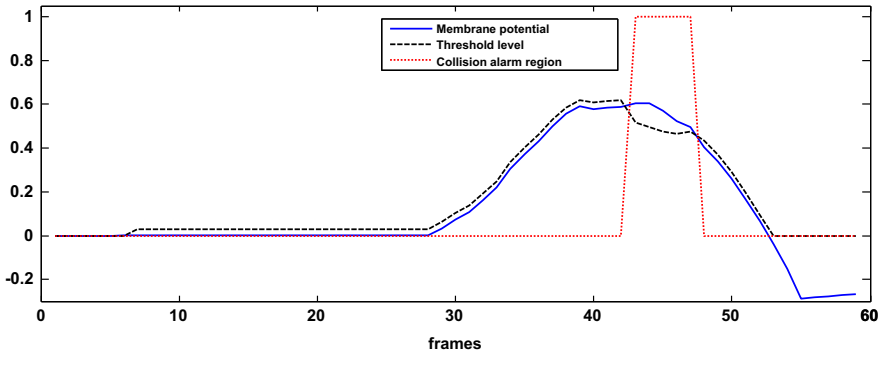

(4) video 4

Fig. 5. Collision regions and output curves of AFVNN's membrane potential and AVCDM's threshold.

can capture some information on the walker. In Fig. 7(1) below, the membrane potential curve shows that the person appears in the field of view from frame 1 to frame 41, which consists with the practical scene. After frame 41, the person appears in the edge of the wide field of view. We prescribe that when a moving object appears in the front of the field of view, collision alarms are sent by AVCDM, even if the object is not approaching the camera. On the other hand, since AFVNN gets a strong membrane potential at

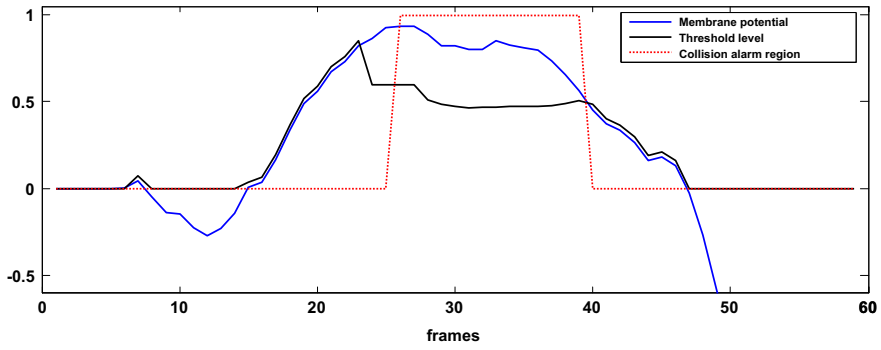

(1) video 5

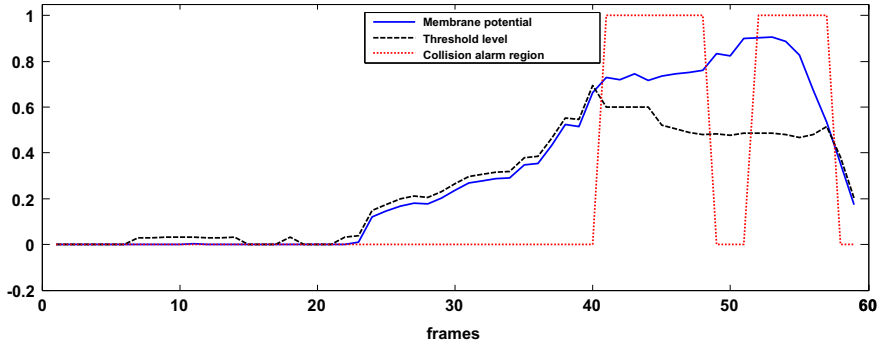

(2) video 6

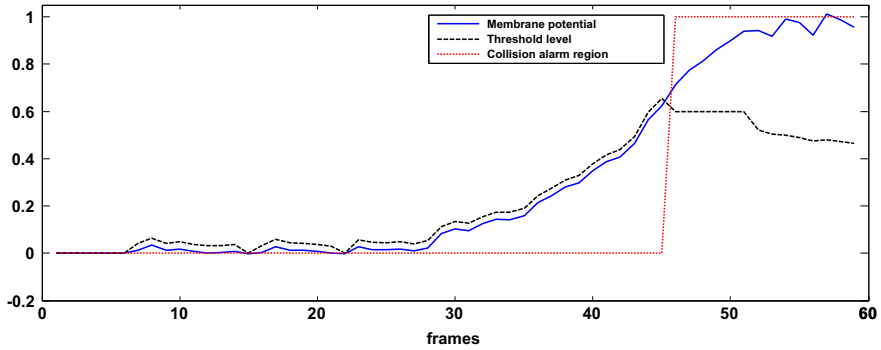

(3) video 7

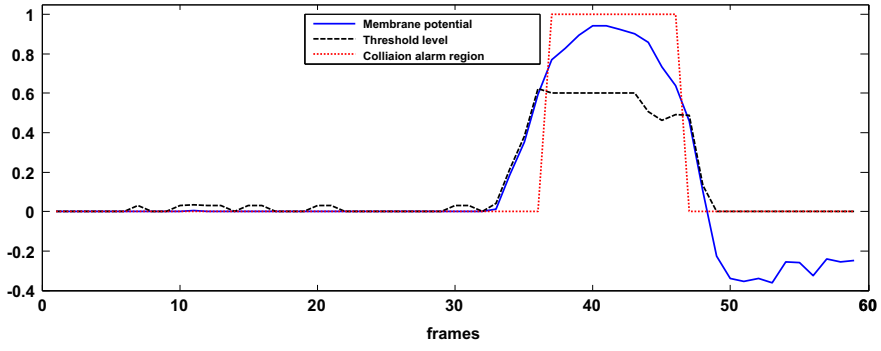

(4) video 8

Fig. 6. Collision regions and output curves of AFVNN's membrane potential and AVCDM's threshold.

frame 35, the threshold curve makes AVCDM transmit the collision alarm information within frames 31 and 37. The collision alarm region is at frames 31–38. These results illustrate that AFVNN can correctly identify the intensity of motion of the walker in the wide field of view, and the collision detection mechanism can correctly send collision alarms and transmit the collision region.

Video sequence 10 provides some clues arisen from the process which a practical car translates and collides an inflatable car. In the practical scene, the driving car turns anticlockwise or clockwise at frames 59–67; correspondingly, AFVNN's output curve presents big fluctuation within frames 55 and 65. In such case, no collision alarms appear in the scene, which is also demonstrated by Fig. 7(2).

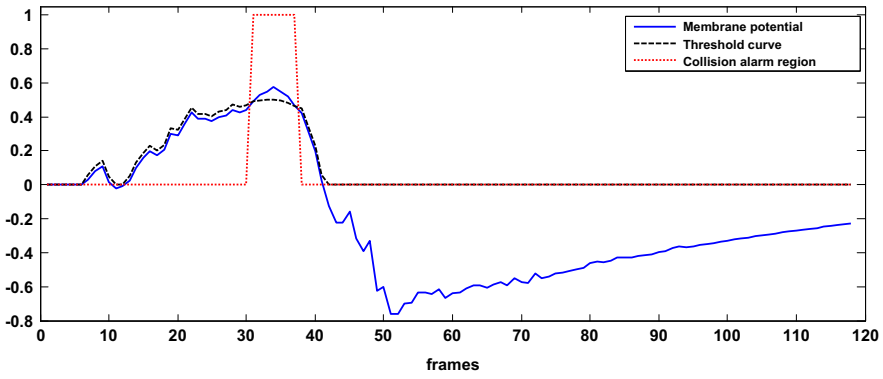

(1) video 9

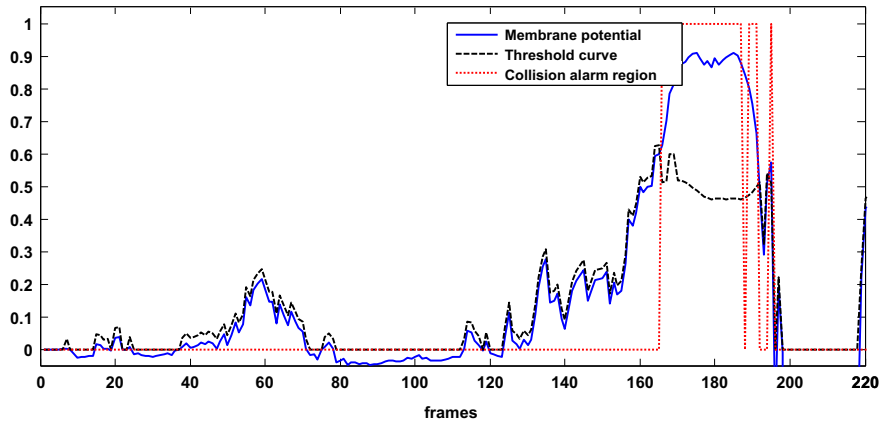

(2) video 10

Fig. 7. Collision regions and output curves of AFVNN's membrane potential and AVCDM's threshold.

After frame 110 in the sequence, the driving car will collide with the inflated ball at a high speed. Especially, after frame 190, collision takes place. For such scene, AVCDM can provide a correct threshold curve to produce collision alarms and the collision region. Additionally, we note that after collision takes place within frames 190 and 200, AFVNN's membrane potentials reduce dramatically, and thus collision alarms elapse gradually. Experimental results illustrate that under the above car collision environment, AVCDM can successfully execute collision detection. More importantly, the practical car drives with turnover within frames 46 and 64, this phenomenon causes that AFVNN's outputs present small fluctuation within such frames. Interestingly, in such case AVCDM does not send a false collision alarm.

Totally, collision detection is a fundamental ability for many of the flying insects. This ability may be achieved via difference mechanisms in different insect species [31,32]. Our research in this paper demonstrated that a collision detection system inspired by the fly works well.

6.3. Comparative analysis

A reported competitive collision detection system, simply written as artificial visual neural system (AVNS) proposed by Yue [33] is adopted to compare with AVCDM, in which the neural network in AVNS is represented by artificial locust visual neural network (ALVNN). It bases on the inner structure of the lobula giant movement detector (LGMD) in the locust visual system, and meanwhile its parameter settings are the same as those in [33]. After executing on all the above video sequences in Section 6.1, AVNS acquires the collision regions in Table 3 and the curves of collision detection. We only draw some curves as in Figs. 8 and 9 below to illustrate AVNS' characteristics, due to the limited space of page.

Table 3
Collision regions found by AVNS.

Video no.	AVLNS's collision region (frames)	Success rate (%)	Video no.	AVLNS's collision region (frames)	Success rate (%)
1	15–19, 24, 39–58	100	6	44–60	100
2	31–40, 45–59	100	7	49–54	100
3	No	0	8	38–44	100
4	38–49	100	9	36–39	100
5	20–28, 33–53	50	10	173–189, 194	100

Tables 2 and 3 hint that AVNS and AVCDM have some similar characteristics and also significant differences when deciding the collision regions for the above video sequences. Through all the above videos but video sequences 3 and 5, AVNS can correctly produce collision alarm signals, once an object is approaching the video camera. We also notice that it fails to find the unique collision region in video sequence 3, maybe because the black ball bounces at a high velocity and the initial threshold value (0.88) in the threshold mechanism is large. Additionally, AVNS can successfully identify the collision region (frames 20–38) for video sequence 5, but produces a false collision source (frames 39–53). Even if so, ALVNN is still an alternative and potential collision detection system solving real-world collision scenes. By comparison, the results in Table 2 show that AVCDM is of potential value for collision region detection in complex dynamic environments.

Graphically by Figs. 5–7, the curves of membrane potential acquired by AFVNN are relatively smooth, because Eqs. (4) and (7)

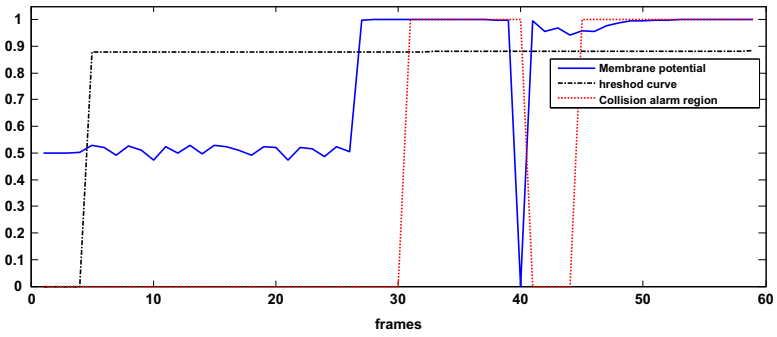

(1) video 2

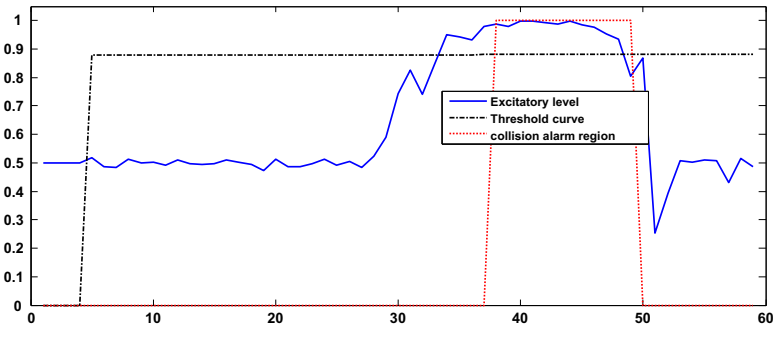

(2) video 4

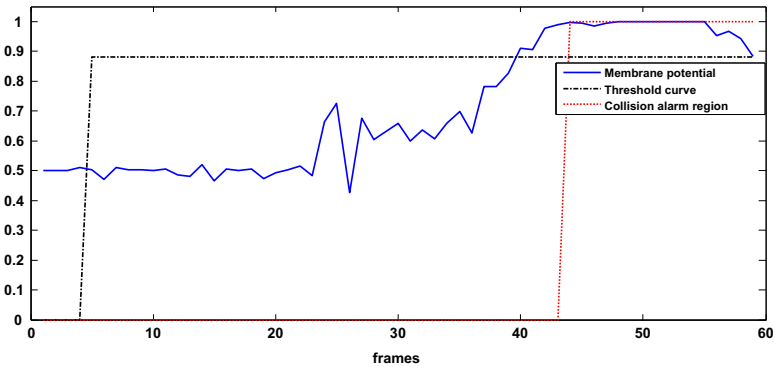

(3) video 6

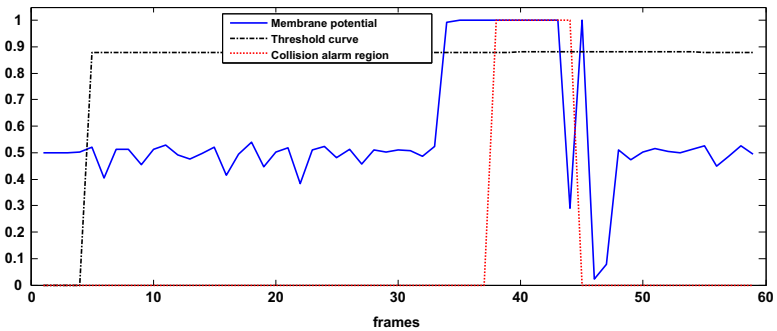

(4) video 8

Fig. 8. AVNS: collision regions and output curves of membrane potential and threshold.

can partially prevent the outputted membrane potentials from background noises. Each of them can reflect reasonably the characteristics of motion of the object emerging in the field of view, while making a large change once such object is close to the camera. For example, video sequence 2 includes two collision regions in the wide field of view (frames 29–36 and 48–60); once

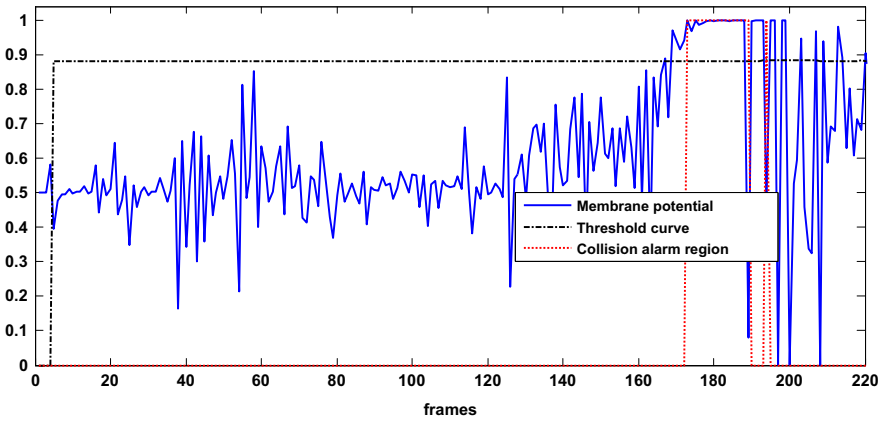

Fig. 9. AVNS: collision regions and output curves of membrane potential and threshold for Video 10.

the collision regions emerge, AFVNN outputs high membrane potentials. Such property also appears in ALVNN, namely the membrane potentials outputted by ALVNN can also describe the characteristics of the moving object, e.g., see Figs. 8 and 9. However, ALVNN's output curves are not smooth, which easily makes AVNS produce false collision alarms because of noisy influence. Additionally, the threshold curves in Figs. 8 and 9 illustrate that the threshold mechanism in AVNS ensures the threshold value at each moment to change within a small scope. Conversely, AVCDM makes the threshold curves change within a wide scope. Namely, when some object is approaching a robot or camera, the differences between the threshold values and AFVNN's outputs are large. This help AVCDM send correct collision alarm signals.

7. Conclusions

With the increasing requirement of real-world collision detection for driving cars, bio-vision based neural network will become popular. Thus, this work suggests one artificial collision detection system (AVCDM) capable of effectively sending collision alarms and identifying collision regions for driving cars, inspired by the interactive internal structures and vision processing functions of fly visual systems. Especially, one simple artificial visual neural network is developed to capture online the performance characteristics produced by a moving object approaching a camera or robot, by simulating the process of fly visual information processing. In such neural network, a shunting inhibition model is used to estimate the activities of different kinds of cells. Meanwhile, depending on such neural network, one collision detection mechanism is designed carefully to transmit collision detection signals; one threshold detection mechanism, capable of adapting to multiple kinds of complex video scenes, plays an important role in deciding when and whether a collision alarm happens. Experimentally, the comparative results demonstrated that (1) fly visual neural systems are a striking bio-inspiration for studying computationally collision detection tools, (2) AFVNN can effectively present the performance characteristics for a moving object to approach a camera or robot, and (3) AFVNN-based AVCDM can avoid false collision alarms; once a scene includes collisions, such detection system can send right collision alarms and collision regions even if video scenes become complex.

Acknowledgments

The authors are grateful to the anonymous reviewers for their helpful comments. They also thank the editors of this work for their support. This work is partially supported by the Doctoral Fund of Ministry of Education of the People's Republic of China (20125201110003), EU FP7 HAZCEPT (318907) projects and the National Natural Science Foundation, PR China, NSFC (61065010).

References

[1] D.A. Clark, L. Bursztyn, M.A. Horowitz, et al., Defining the computational structure of the motion detector in Drosophila, Neuron 70 (2011) 1165–1177.
[2] A. Borst, T. Euler, Seeing things in motion: models, circuits, and mechanisms, Neuron 71 (2011) 974–994.
[3] M.S. Maisak, J. Haag, G. Ammer, et al., A directional tuning map of Drosophila elementary motion detectors, Nature 500 (2013) 212–216.
[4] S.Y. Takemura, A. Bharioke, Z.Y. Lu, et al., A Visual motion detection circuit suggested by Drosophila connectomics, Nature 500 (2013) 175–183.
[5] H. Eichner, M. Joesch, B. Schnell, et al., Internal structure of the fly elementary motion detector, Neuron 70 (2011) 1155–1164.
[6] J.K. Douglass, N.J. Strausfeld, Visual motion detection circuits in flies: peripheral motion computation by identified small-field retinotopic neurons, J. Neurosci. 15 (8) (1995) 5596–5611.
[7] A.K. Warzecha, R. Rosner, J. Grewe, Impact and sources of neuronal variability in the fly's motion vision pathway, J. Physiol. 107 (2013) 26–40.
[8] S. Rajesh, D. O'Carroll, D. Abbott, Elaborated Reichardt correlator for velocity estimation tasks, in: D.V. Nicolau, A.P. Lee (Eds.), Proceedings of the Biomedical Applications of Micro- and Nanoengineering, vol. 4937, 2002, pp. 241–253.
[9] C.W.G. Clifford, M.R. Ibbotson, Fundamental mechanisms of visual motion detection: models, cells and functions, Prog. Neurobiol. 68 (2003) 409–437.
[10] C.M. Higgins, V. Pant, An elaborated model of fly small-target tracking, Biol. Cybern. 91 (2004) 417–428.
[11] B. Babies, J.P. Lindemann, M. Egelhaaf, et al., Contrast-independent biologically inspired motion detection, Sensors 11 (2011) 3303–3326.
[12] H.G. Meyer, J.P. Lindemann, M. Egelhaaf, Pattern-dependent response modulations in motion-sensitive visual interneurons – a model study, PLoS One 6 (7) (2011) e21488. http://dx.doi.org/10.1371/journal. pone. 0021488.
[13] C.M. Higgins, J.K. Douglass, N.J. Strausfeld, The computational basis of an identified neuronal circuit for elementary motion detection in Dipterous insects, Visual Neurosci. 21 (2004) 567–586.
[14] R.A. Zuley, C.M. Higgins, Contrast saturation in a neuronally-based model of elementary motion detection, Neurocomputing 65–66 (2005) 173–179.
[15] E. Nakamura, M. Ichimura, K. Sawada, Fast global motion estimation algorithm based elementary motion detectors, in: Proceedings of the International Conference on Image Processing, vol. 2, 2002, pp. 297–300.
[16] F. Ruffier, N. Franceschini, Optic flow regulation: the key to aircraft automatic guidance, Robot Auton. Syst. 50 (2005) 177–194.
[17] B. Gui, Performance Estimation of Oversampled Bio-inspired Velocity Estimator Based on Reichardt Correlator (M.Sc. Degree thesis), Northwestern Polytechnical Universty, China, 2010.
[18] R.O. Dror, D.C. O'Carroll, S.B. Laughlin, Accuracy of velocity estimation by Reichardt correlators, Opt. Soc. Am. 18 (2) (2001) 241–252.
[19] H.Y. Wu, K. Zou, T.G. Zhang, A. Borst, K. Kühnlenz, Insect-inspired high-speed motion vision system for robot control, Biol. Cybern. 106 (8–9) (2012) 453–463.
[20] L. Zhang, T.G. Zhang, H.Y. Wu, et al., Visual flight control of a quadrotor using bioinspired motion detector, Int. J. Navig. Observ. (2012), http://dx.doi.org/10.1155/2012/627079 (Article ID 627079).
[21] J.W. Aptekar, P.A. Shoemaker, M.A. Frye, Figure tracking by flies is supported by parallel visual streams, Curr. Biol. 22 (2012) 482–487.
[22] H.J. Sun, L. Liu, A. Guo, A neurocomputational model of figure-ground discrimination and target tracking, IEEE Trans. Neural Netw. 10 (4) (1999) 860–884.

[23] J.M. Misserler, F.A. Kamangar, A neural network for pursuit tracking inspired by the fly visual system, Neural Netw. 8 (3) (1995) 463–480.
[24] V. Pant, C.M. Higgins, Tracking improves performance of biological collision avoidance models, Biol. Cybern. 106 (4) (2012) 307–322.
[25] M.E. Basch, R.I. LÖrincz, D.G. Cristea, et al., A bio-inspired collision avoidance system concept for people with visual disabilities, Int. J. Syst. Appl. Eng. Dev. 6 (5) (2011) 701–709.
[26] S.B.I. Badia, P.F.M.J. Verschure, A collision avoidance model based on the Lobula Giant Movement Detector (LGMD), in: Proceedings of the International Joint Conference on Neural Networks IJCNN'04, Budapest, Hungary, 2004, pp. 1757–1761.
[27] J. Xu, Y.F. Yin, H. Man, et al., Feature selection based on sparse imputation, in: Proceedings of the 2012 International Joint Conference on Neural Networks (IJCNN), Brisbane, QLD, Australia, 10–15 June 2012, pp. 1–7.
[28] R. Stafford, R.D. Santer, F.C. Rind, A bio-inspired visual collision detection mechanism for cars: combining insect inspired neurons to create a robust system, Bio Syst. 87 (2007) 164–171.
[29] R.R. Harrison, A biologically inspired analog IC for visual collision detection, IEEE Trans Circuits Syst. – I 52 (11) (2005) 2308–2318.
[30] S.G. Yue, F.C. Rind, A synthetic vision system using directionally selective motion detectors to recognize collision, Artif Life 13 (2) (2007) 93–122.
[31] S.G. Yue, F.C. Rind, Evolutionary comparison of visual neural subsystems for collision recognition, IEEE Trans. Auton. Ment. Dev. 5 (2) (2013) 173–186.
[32] S. Yue, F.C. Rind, Postsynaptic organization of directional selective visual neural networks for collision detection, Nuerocomputing 103 (2013) 50–62.
[33] S.G. Yue A collision detection system for a mobile robot inspired by the locust visual system, in: Proceedings of the 2005 IEEE International Conference on Robotics and Automation, ICRA 2005, Barcelona, Spain, April 18–22 2005.

Zhuhong Zhang received his M.S. degree from the Department of Mathematics, Guizhou University, China, and Ph.D. degree from the College of Automation, Chongqing University, China. Currently, he is a Professor at the Guizhou University and an Associate Editor for Journal of Applied Soft Computing. His main areas of interests include uncertain programming, evolutionary algorithms, immune optimization, and signal simulation. He has also published more than 50 journal and conference papers in control theory, intelligent computing, project planning management and neural network.

Shigang Yue received his Ph.D. and M.Sc. degrees from the Beijing University of Technology, and his B.Eng. degree from the Qingdao Technological University. Currently, he is a Professor of Computer Science in the Lincoln School of Computer Science, University of Lincoln, United Kingdom. His research interests are mainly within the field of artificial intelligence, computer vision, robotics, brains, and neuroscience. He has published more than 60 journal and conference papers in computer vision, artificial life, neural systems, neural evolution, vehicle collision detection, robotic navigation, robotic manipulation skills and dynamic simulations, many of them are in top tier high impact journals.

Guopeng Zhang received his B.S. degree from the Zhejiang University, China. He is pursuing the Master degree at the Institute of Microelectronics, Tsinghua University. He also works as a Research Assistant on specific chip design for Computational Intelligence Laboratory at the University of Lincoln, UK. His research interests include biologically inspired vision chip, VLSI design in parallel computing and artificial neural networks for perception.